Effects of a nonlinear damping force in synchrotrons with electron cooling

D.D. Caussyn,[1] M. Ball,[1] J. Budnick,[1] G. East,[1] M. Ellison,[1] B. Hamilton,[1] K. Hedblom,[3] X. Kang, S.Y. Lee,[1] D. Li,[1] J.Y. Liu,[1] K.Y. Ng,[2] A. Riabko,[1] L. Wang,[1] and Y. Wang[1]
[1]*Indiana University Cyclotron Facility, 2401 Milo B. Sampson Lane, Bloomington, Indiana 47408*
[2]*Fermilab, P.O. Box 500, Batavia, Illinois 60510*
[3]*Uppsala University, The Svedberg Laboratory Box 533, S-75121, Uppsala, Sweden*
(Received 27 September 1994)

The longitudinal dynamics of a stored proton beam bunch, under the influence of a nonlinear damping force produced by electron cooling, was studied experimentally. The effect of the nonlinear damping force was explored by varying the relative velocity between the cooling electrons and the stored protons. Maintained longitudinal oscillations developed, which grew rapidly once a critical threshold in the relative velocity was exceeded. The bifurcation of a fixed point into a limit cycle is also known as a Hopf bifurcation. Comparisons of experimental data with numerical simulations and analytical calculations are made. Implications for cooled beam acceleration will be discussed.

PACS number(s): 29.27.Bd, 41.75.−i, 03.20.+i, 05.45.+b

I. INTRODUCTION

The Indiana University Cyclotron facility (IUCF) Cooler Ring was the first of many similar accelerator storage rings designed specifically to employ electron cooling to produce high quality medium energy ion beams for use in nuclear research [1]. The electron cooling mechanism has been used extensively in multiturn kick injection where the newly injected particles are cooled to the stack tail, in counteracting the phase space growth during the internal target experiments, and in increasing the lifetime of the stored beam by balancing diffusion processes. For a beam of 45-MeV protons, the equilibrium 95% transverse emittance, or phase space area, is about 0.3π mm mrad with a relative momentum spread full width at half maximum (FWHM) of about 1×10^{-4}. The motion of a beam bunch with this small an emittance can closely simulate single-particle motion. Several experiments studying transverse motion near betatron resonances [3] have demonstrated this advantage.

Recently, we have applied many of the same techniques for studying transverse motion on a turn-by-turn basis to investigate longitudinal motion, particularly the parametric resonances that occur when the rf phase or voltage is modulated [4]. In the course of making these measurements we have also observed driven, or maintained, sometimes dipolelike longitudinal oscillations. These maintained driven oscillations were generated by the damping force of the electron cooling when the energy of the rf synchronous particle differed from the electron beam energy. A similar effect has been previously observed and identified as rigid dipole oscillations in Ref. [5]; however, there has been no detailed study of this phenomenon.

A possible effect of this instability is to heat a stored proton beam; consequently it has important implications for injection schemes in which the electron cooling is used to cool newly injected beam into a previously stored proton beam. It may also be relevant for determining how the energy of cooling electrons is changed as the proton beam is accelerated. Since the electron cooling is effective only when the relative velocity between the proton and the electron beams is small compared with the velocity spread of the electron beam, beam dynamics studies on the effects of a nonlinear damping force are important for improving beam manipulation performance. More broadly this effect is of interest in understanding any pendulumlike system with nonlinear damping.

In this paper we report experimental results from studying beam motion when the energy of the synchronous proton is varied while holding the electron energy constant. These experimental results are compared with results from numerical simulations, where the onset of the limit cycle instability is related to the temperature of the electron beam. Near the threshold of the instability, analytic solutions can be obtained by using harmonic linearization and perturbative expansion methods. We also report the results obtained from harmonically modulating the electron beam energy. This process, equivalent to another parametric resonance created by rf phase modulation, can be used to measure the cooling rate for particles with small amplitude phase oscillations. We organize this paper as follows. In Sec. II, synchrotron motion in the presence of electron cooling will be briefly reviewed. In Sec. III, experimental methods in studying the synchrotron motion with nonlinear damping will be discussed and experimental results will be compared with numerical simulations. The conclusion is given in Sec. IV.

II. REVIEW OF SYNCHROTRON MOTION WITH ELECTRON COOLING

Since its discovery in 1945 by McMillan and Veksler [2], synchrotron motion has come to be relatively well understood. However, synchrotron motion in a system

with electron cooling has received relatively little attention. Ideally, electron cooling adds a damping force to the system and thus synchrotron motion is similar to that of a damping pendulum.

Longitudinal motion in a synchrotron is characterized by the phase ϕ, which is the phase of a particle relative to the rf cavity voltage, and its conjugate momentum variable δ, which is the fractional momentum deviation of the particle from that of the synchronous particle, i.e., the particle that arrives at the same time each revolution relative to the rf voltage. The difference equations describing the longitudinal motion are

$$\delta_{n+1} = \delta_n - \frac{2\pi\nu_s^2}{h\eta}(\sin\phi_n - \sin\phi_s) - f(\delta_n), \tag{1}$$

$$\phi_{n+1} = \phi_n + 2\pi h\eta\delta_{n+1}, \tag{2}$$

where η is the phase slip factor, ϕ_s is the phase of the synchronous particle, which for a stored beam is 0°, h is the harmonic number, $f(\delta)$ is the damping force, provided in our case by electron cooling, ν_s is the small amplitude synchrotron tune at a zero synchronous phase, and the subscripts n refer to the revolution number. The synchrotron tune ν_s is related to the rf cavity voltage $V_{\rm rf}$ by $\nu_s = \sqrt{h|\eta|eV_{\rm rf}/2\pi E\beta^2}$, where e, βc, and E are, respectively, the charge, the speed, and the total energy of the proton. The angular synchrotron frequency is given by $\omega_s = \omega_0\nu_s$, where ω_0 is the angular revolution frequency. Also, the stable region of the longitudinal phase space provided by the rf cavity voltage is called the rf bucket.

A. Damping force

The damping force $f(\delta)$ produced by the electron cooling is the result of a statistical exchange of energy in Coulombic collisions between the protons and relatively cold electrons as they travel together at the same velocity in the accelerator. In practice, electron cooling in synchrotrons is normally done in relatively short straight sections due to cost and space limitations. At IUCF the electron beam is mixed with the proton beam for a distance of only 2.2 m or about 2.5% of the circumference of the ring. The electron beam radius is about 1.27 cm and the cathode temperature is about 1300° or $kT_{\rm cath} = 0.11$ eV [5], where k is the Boltzmann constant. The maximum electron beam current is 4 A.

Heuristically, the longitudinal damping force can be viewed as follows. In the rest frame of electrons, protons with higher or lower velocities than that of nearly equal-speed electrons have to travel forward or backward through the cold electron cloud in the electron cooling section. Since the charged ions lose energy in passing through the electron cloud, the protons will be slowed down relative to the rest frame of the electron beam. For an electron beam current of 1 A, the effective electron cloud target thickness is about 3.0×10^{10} electrons/cm^2, i.e., the density of the electron is about $n = 1.4 \times 10^{14}$ electrons/m^3. Because the velocities of the electrons and protons are nearly equal, this very thin target of cold electrons can efficiently damp the proton beam oscillations and sustain the diffusion process of a fixed internal target having a thickness of about 10^{16} charges/cm^2 [6]. In our experiments, the cooling electron beam current was normally 0.75 A.

Generally, the damping force is a nonlinear function of the relative velocity $v_{\rm rel}$ between protons and the electron beam. Let δ be the fractional momentum deviation of a proton from the synchronous particle and δ_e the fractional momentum deviation of a proton traveling at the same velocity as the electrons from the synchronous particle. The relative velocity $v_{\rm rel}$ between a proton and the cooling electrons in the laboratory frame is given by

$$v_{\rm rel}^{\rm lab} = (\delta - \delta_e)\beta c/\gamma^2, \tag{3}$$

where β and γ are the usual relativistic factors for the synchronous particle and c is the speed of light. In the rest frame of the electrons, the relative velocity is

$$v_{\rm rel}^{\rm rest} = \gamma_e^2 v_{\rm rel}^{\rm lab}/(1 - \gamma_e^2\beta_e v_{\rm rel}^{\rm lab}/c), \tag{4}$$

where γ_e and β_e are relativistic factors for the electron beam. Normally, for $|v_{\rm rel}^{\rm lab}| \ll c$ and $\gamma_e \approx \gamma$, we have

$$v_{\rm rel}^{\rm rest} \approx (\delta - \delta_e)\beta c. \tag{5}$$

Hereafter we will drop the superscript specifying the reference frame with $v_{\rm rel}^{\rm rest} \to v_{\rm rel}$ and for all future references the relative velocity will be understood to be in the electron rest frame.

Assuming an electron beam with an isotropic phase space Maxwellian velocity distribution, the damping force in the nonmagnetized binary collision theory is given by [7]

$$f(\delta) = K\left(\frac{v_{\rm rel}}{\sigma_e}\right)^{-2}\frac{\sqrt{\pi}}{2}\left\{\mathrm{erf}\left(\frac{v_{\rm rel}}{\sigma_e}\right) - \frac{2}{\sqrt{\pi}}\left(\frac{v_{\rm rel}}{\sigma_e}\right)\exp\left[-\left(\frac{v_{\rm rel}}{\sigma_e}\right)^2\right]\right\}, \tag{6}$$

where σ_e is the rms velocity spread of the electron beam, which is presumed to have a Gaussian distribution, and K is a constant that is approximately independent of the relative velocity. Expressed in terms of the fractional momentum, the equation for the damping force becomes

$$f(\delta) = \frac{4\pi\alpha\Delta_e}{\omega_0}g(\zeta), \tag{7}$$

where $\Delta_e = \sigma_e/\beta c$, $\zeta = (\delta - \delta_e)/\Delta_e$, α is the $1/e$ damping rate for small relative velocities with units s^{-1}, and $g(\zeta)$ is a kinematic factor given by

$$g(\zeta) = \frac{3\sqrt{\pi}}{4\zeta^2}\left[\mathrm{erf}(\zeta) - \frac{2\zeta}{\sqrt{\pi}}e^{-\zeta^2}\right]. \tag{8}$$

This kinematic factor has the following properties:

$$g(-\zeta) = -g(\zeta), \quad g(\zeta)|_{\zeta\to 0} \to \zeta,$$
$$g'(\pm 0.97) \approx 0, \quad g(\pm 0.97) \approx \pm 0.57.$$

Asymptotically, $g(\zeta)|_{\zeta\to\infty} \approx \frac{3\sqrt{\pi}}{4\zeta^2}$.

B. Effective electron temperature

The effective temperature of the electron beam is related to the rms electron velocity spread by

$$kT_{\|\text{eff}} = \frac{1}{2}m_e\sigma_e^2 = \frac{1}{2}m_e\beta^2c^2\Delta_e^2. \quad (9)$$

Theoretically, the electron temperature is related to the cathode temperature of the electron gun by (see p. 185 of Ref. [7])

$$kT_{\|\text{eff}} = \frac{1}{4}\left(\frac{\sigma_U}{U_{\text{cath}}} + \frac{kT_{\text{cath}}}{E_0}\right)^2 E_0 + 2m_ec^2\frac{r_e}{r_{\text{av}}}, \quad (10)$$

where U_{cath} is the voltage of the acceleration column, $E_0 = eU_{\text{cath}}$ is the nominal electron energy, σ_U is the voltage ripple of the acceleration column, r_e is the classical electron radius, and r_{av} is the average radius of the sphere occupied by an electron. Typically, we have $\sigma_U < 3$ V, and $r_{\text{av}} \approx 1.2\times10^{-5}$ m at 1 A of electron beam current, and thus the resulting longitudinal effective temperature can be as small as 0.0003 eV, dominated by the voltage ripple and the static Coulomb potential term in Eq. (10). Because of the adiabatic acceleration, the longitudinal effective electron temperature is much smaller than that of the cathode temperature, which is of the order of $kT_{\text{cath}} = 0.11$ eV. However, there is no adiabatic damping in the transverse phase space, so the effective transverse temperature remains 0.11 eV.

In machines where the electron beam is magnetically confined by a solenoidal field, as it is in the IUCF Cooler Ring, the damping force can be enhanced by an effect called magnetized cooling. Magnetized cooling can be substantial for small relative velocities, where electrons are trapped in magnetic field lines, the effective longitudinal and transverse cooling rates can be greatly enhanced. However, for this effect to become important, there must be a rather precise alignment of the electron and the proton beams, which under normal operating conditions is unlikely (see p. 117 of Ref. [5]). During our experiments, the electron cooling system was adjusted to optimize the cooling rate and the lifetime of the proton beam without making a painstaking effort to precisely align the proton and the electron beams. Therefore, we assume that the damping force is given by the nonmagnetized theory of Eq. (7), where parameters α and Δ_e are used to represent the effective damping rate and electron beam temperature.

In Fig. 1, sketches of the damping force for two different cases are shown. In Fig. 1(a) the damping force $f(\delta)$ is shown for the case where the electron velocity is the same as the velocity of the synchronous particle, i.e., $\delta_e = 0$. In this case the damping force is zero for a particle at the center of the rf bucket, where the rf force is zero. In Fig. 1(b) the damping force $f(\delta)$ is shown for the case where the electron velocity is much different from the velocity of the synchronous particle, i.e., $\delta_e \neq 0$. In this case the damping force is nonzero for a particle at the center of the rf bucket, where the rf force is zero. More importantly, the slope of the damping force at the center of the bucket has changed sign. As we shall discuss later, this leads to an instability when the synchronous particle is slightly displaced from the center of the rf bucket.

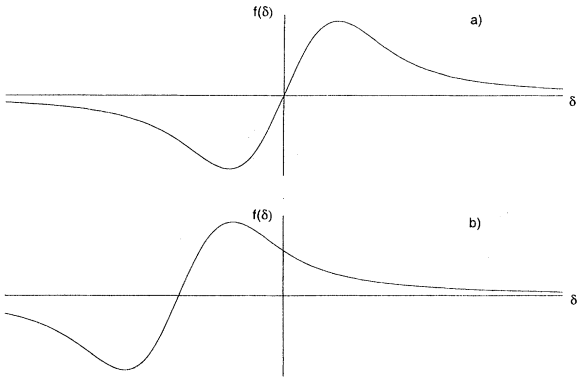

FIG. 1. (a) Damping force $f(\delta)$ plotted as a function of the momentum deviation δ of the proton beam from the synchronous particle. (b) $f(\delta)$ plotted for the case where the electron beam has a velocity different from the velocity of the synchronous particle.

III. EXPERIMENTAL METHODS AND RESULTS

The IUCF Cooler Ring is a hexagonal shaped storage ring with a circumference of 86.8 m. The experiment was done with a 45-MeV proton beam injected and then stored in a 10-s cycle time. After 5 s from the start of the cycle, the six-dimensional phase space coordinates were digitized at ten-revolution intervals for 16 384 points. The nominal rf cavity frequency was 1.031 68 MHz with the harmonic number $h = 1$, i.e., the rf cavity frequency was equal to the beam revolution frequency. At this energy, the phase slip factor η of the Cooler Ring was about -0.86. The beam was a single bunch of about 3×10^8 protons with a typical length of about 60 ns (or 5.4 m) FWHM for a rf peak voltage of about 41 V. Since measurements of longitudinal motion were being made, the phase lock feedback loop for the rf, which is normally on, was switched off. Damping of a synchrotron oscillation while operating under these conditions occurred entirely due to the electron cooling.

The phase of the beam was determined using a phase detector having a range of 720° to measure the relative phase between the signal from a pickup coil in the rf cavity and a sum signal from a beam position monitor (BPM) after it had been passed through a 1.4-MHz low pass filter. The momentum deviation of the beam was found from changes in the position of the beam closed orbit Δx_{CO}, which was measured with a BPM in a region of high dispersion. The fractional momentum deviation δ could then be determined using the relation $\delta = \Delta x_{\text{CO}}/D_x$, where the dispersion D_x was measured to be 3.9 m. The position signal was passed through a 3-kHz low pass filter to remove effects of coherent betatron oscillations. Both the δ and the phase signals were digitized using our data acquisition system, which has been described elsewhere [3].

Driven longitudinal oscillations were produced and studied for two very different circumstances. In one case,

driven motion was produced by harmonically modulating the electron beam energy and, for the other case, by changing the relative velocity between the electron beam and the synchronous particle. In the latter case, the effects of the nonlinear damping force played a crucial role in generating coherent particle oscillations.

A. Harmonic modulation of damping force

For small relative velocities between the proton beam and the electron beam, the linearized damping force is given by

$$f(\delta) = \frac{4\pi\alpha}{\omega_0}(\delta - \delta_e). \tag{11}$$

Thus the damping force can be modulated by harmonically modulating δ_e, or equivalently the electron energy. This was accomplished by resistively adding a small modulating signal to the much larger control signal for the high voltage power supply (HVPS). The HVPS provides the voltage drop for electrons in the electron cooling system, so the applied voltage V for the electrons becomes $V = V_0 + \hat{V}\sin\nu_m\theta$, where V_0 is the applied voltage to maximize the damping force, $\hat{V}$ is the magnitude of the voltage modulation, ν_m is the modulation tune, which is the ratio of the modulation frequency ω_m to ω_0, and the orbital angle $\theta = \omega_0 t$ serves as the time variable. If V_0 maximizes the damping force, which for our experiment was at a nominal value of 24 508 V, then the fractional momentum deviation of the electron beam δ_e is given by $\delta_e = \hat{\delta_e}\sin\nu_m\theta$, where $\hat{\delta_e} = e\hat{V}/E_e\beta^2$ is the magnitude of the modulation with E_e as the total electron energy. So in this case the expression for the damping force becomes

$$f(\delta) = \frac{4\pi\alpha}{\omega_0}(\delta - \hat{\delta_e}\sin\nu_m\theta). \tag{12}$$

With this harmonically modulated damping force, Eqs. (1) and (2) become

$$\delta_{n+1} = \delta_n - \frac{2\pi\nu_{s_0}^2}{h\eta}(\sin\phi_n - \sin\phi_s) - 2\pi\lambda(\delta_n - \hat{\delta_e}\sin\nu_m\theta), \tag{13}$$

$$\phi_{n+1} = \phi_n + 2\pi h\eta\delta_{n+1}, \tag{14}$$

where $\lambda = 2\alpha/\omega_0$. The *damping decrement*, defined as the damping per revolution $\frac{2\pi\alpha}{\omega_0}$, is given by $\pi\lambda$. For a stored beam with $\phi_s = 0$, the synchrotron equation of motion becomes

$$\ddot{\phi} + \lambda\dot{\phi} + \nu_s^2\sin\phi = h\eta\lambda\hat{\delta_e}\sin\nu_m\theta, \tag{15}$$

where the dots indicate derivatives with respect to θ. Thus a harmonic modulation to the damping force is equivalent to the rf phase modulation with an effective modulation amplitude a given by [4]

$$a = \frac{h|\eta|\lambda\hat{\delta_e}}{\nu_m^2} = \frac{\lambda}{\nu_m}\left(\frac{h|\eta|e\hat{V}}{\nu_m\beta^2E_e}\right), \tag{16}$$

where $\hat{V}$ is the amplitude of the HVPS modulation amplitude. In our experimental setting, we had typically $a \approx 5.71\times10^{-7}\alpha\hat{V}$ with α in s^{-1} and $\hat{V}$ in volts. For $\alpha \le 40\ s^{-1}$ and $\hat{V} \le 4$ V, the resulting effective modulation amplitude was $a \le 10^{-4}$ rad.

To first order, the steady-state solution to the equation of motion of Eq. (15) is

$$\phi = \hat{\phi}\sin(\nu_m\theta + \chi), \tag{17}$$

where $\hat{\phi}$ and χ are given implicitly by

$$[-\hat{\phi}\nu_m^2 + 2\nu_s^2J_1(\hat{\phi})]^2 + (\lambda\hat{\phi}\nu_m)^2 = (a\nu_m^2)^2, \tag{18}$$

$$\tan\chi = \frac{\lambda\hat{\phi}\nu_m}{\hat{\phi}\nu_m^2 - 2\nu_s^2J_1(\hat{\phi})}. \tag{19}$$

Here J_1 is the first-order Bessel function.

1. Measuring beam response

The measured steady-state solution of Eq. (17) was obtained from our digitized ϕ and δ data after a sufficiently long time for the transient solution to damp out. Experimentally, the phase signal ϕ had a better signal-to-noise ratio than the δ signal. Since the modulation amplitudes were quite small, the observed ϕ signal contained a significant power supply ripple. A digital-filter method was used to eliminate the 60-Hz ripple and its harmonics. We took a fast Fourier transform of the time series of the digitized ϕ data, applied the filter, which consisted of zeroing the frequency components outside the range of

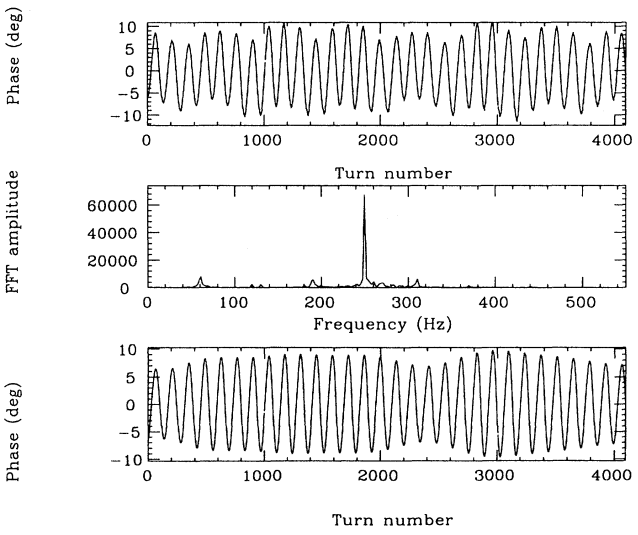

FIG. 2. An example of the filtering done to more accurately determine the beam response. (a) The original time series for the phase measurement. (b) The result of the FFT of the unfiltered time series. (c) The result of the filtered time series.

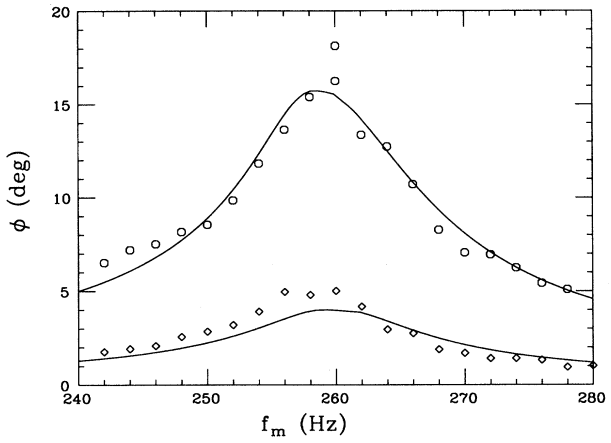

FIG. 3. Plot of the peak phase $\hat{\phi}$ of the steady-state motion for different values of the modulation frequency. The solid lines are the analytical results with the best-fit value for α of 40 Hz.

interest, and then performed an inverse transform. The full width of the digital filter was 70 Hz wide, centered at the nominal synchrotron frequency of 260 Hz. This filter removed all multiples of 60 Hz. The phase oscillations before and after digital filtering for a modulation frequency of 248 Hz are shown at the top and the bottom of Fig. 2. After the filtering was completed, the response $\hat{\phi}$ was obtained from the filtered time series.

2. *Determining the damping parameter α*

The measured phase amplitudes $\hat{\phi}$ for two different HVPS modulation amplitudes $\hat{V}$ are shown in Fig. 3. The diamonds correspond to $\hat{V} = 1.2$ V and the circles correspond to $\hat{V} = 2.5$ V. Using α as an adjustable parameter, the best agreement between the data and Eq. (18) was obtained for $\alpha = 40$ Hz, shown as solid lines in Fig. 3. It is interesting to compare this to a previously determined effective damping rate of $\alpha = 3 \pm 1$ Hz [4], which was determined from the damping rate of phase oscillations with initial amplitudes of about 1 rad. The fact that α varies by over an order of magnitude with amplitude is another manifestation of the nonlinearity of the cooling force. The harmonic modulation of the electron beam energy is an effective probe for measuring the damping parameter α for small phase oscillations.

B. Bifurcation with a nonlinear damping force

To investigate the effect of the nonlinear damping force on synchrotron motion, the electron velocity was displaced from the proton velocity to produce a nonzero relative velocity. This can be achieved in two ways. The most straightforward way would have been to change the electron energy. However, at IUCF the electron energy is changed by changing the HVPS setting digitally in steps of about 4.5 V. This would result in fractional changes in the electron velocity $\Delta\beta/\beta$ in steps of about 9×10^{-5}, which proved to be too coarse a means of changing the relative energy. The other method, the method used for this experiment, is to change the energy of the proton beam. This was done by changing the rf cavity frequency, where a step of 1 Hz resulted in changing the fractional proton velocity by about 1×10^{-6}. If the electron velocity is equal to the proton velocity when the rf cavity frequency is f_0, then the fractional momentum deviation of the electron beam from the proton beam δ_e at the new rf frequency f is given by

$$\delta_e = \frac{(f - f_0)}{\eta f_0}. \tag{20}$$

When the rf frequency is shifted, the beam, which is originally at the center of the rf bucket (i.e., $\delta = 0$ and $\phi = 0$), will be dragged away from the origin and begin to undergo a synchrotron oscillation. If the damping force were linear over the entire range of $v_{\rm rel}$, the proton beam would damp to a new fixed point attractor $\phi_{\rm FP}$, i.e., the synchronous phase angle, where

$$\phi_{\rm FP} \approx \frac{2\alpha}{\omega_0 \nu_s} \frac{h\eta\delta_e}{\nu_s}. \tag{21}$$

This would correspond to the situation where the proton beam was continually losing energy due to the damping force, but with it continually being made back by the rf cavity, or vice versa. Because $\alpha \ll \omega_0 \nu_s$, the resulting $\phi_{\rm FP}$, which is equivalent to the synchronous phase angle ϕ_s of the beam, is very small. This is analogous to a pendulum in a stiff breeze, where the air resistance plays the role of the electron cooling.

In reality, the damping force is a nonlinear function of the relative velocity between the proton and the cooling electrons. The first implication, discussed in Sec. III A 2, is a smaller effective damping rate. More importantly, when the relative velocity is larger than the rms velocity spread of the cooling electrons, the nonlinear damping force can induce large synchrotron oscillations. This section discusses the coherent synchrotron oscillations due to the nonlinear damping force.

1. *Experimental results*

In order to measure the steady-state response of the beam particles, the maximum synchrotron phase amplitude $\hat{\phi}$ and the maximum fractional momentum deviation $\hat{\delta}$ are measured at 5 s after the start of an injection cycle to allow the initial transient oscillations to damp out. A typical result of this measurement is shown in Fig. 4, where two sets of measurements of $\hat{\phi}$ are shown, one using the phase detector previously described and the other using an oscilloscope to measure the separation in time between the extremes in phase oscillations. The small amplitude of phase oscillations shown in Fig. 4 within the rf frequency range of $f - f_0 \in [-260, 120]$ Hz

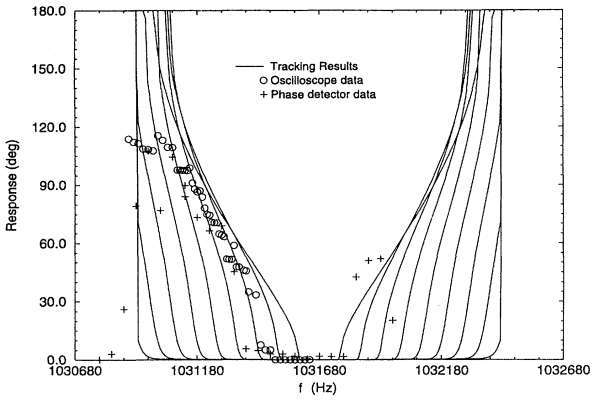

FIG. 4. Plot of the peak phase in degrees of the steady-state motion as the proton energy (rf cavity frequency) is varied. The voltage is 85 V. The solid lines are computer tracking results for Δ_e from 1×10^{-4} to 9×10^{-4}. The onset of the Hopf bifurcation occurs at $\Delta_e \approx 3 \times 10^{-4}$. Note here that the rise of the response amplitude became slower when the rf cavity frequency was below 1.031 18 MHz. This slower response increase may result from a smaller negative resistance term in the damping force.

is consistent with Eq. (21). On the other hand, when the rf frequency is outside this range, the amplitude of synchrotron oscillations becomes very large.

To understand the nature of this instability, the solid lines shown in Fig. 4 are the results of computer simulation using Eqs. (1) and (2) with a damping force given by Eq. (7). The tracking was done for the time equivalent of 60τ, where the damping time is $\tau = 1/\alpha$. Each solid line corresponds to a different electron temperature Δ_e, starting with $\Delta_e = 1 \times 10^{-4}$ for the pair of solid lines nearest the nominal frequency of 1.031 680 MHz and increasing in steps of 1×10^{-4} for each pair of lines as one moves further from the center frequency 1.031 680 MHz. The agreement of the tracking results with the data is not particularly good for large amplitude oscillations, but for small amplitudes the best agreement is obtained when $\Delta_e \approx 3 \times 10^{-4}$. It is clear that a unique feature of the motion is the existence of a threshold for $|v_{\rm rel}|$ (or $|\delta_p - \delta_e|$) beyond which the steady-state motion is no longer a fixed point, but becomes a limit cycle.

The steady-state motion was measured for five other different rf cavity voltages, albeit at various times in a span of about one-half year. Although the electron cooling might not have been identical, the results were qualitatively similar. The results of these measurements are shown in Fig. 5. All but the highest and the lowest rf cavity voltages (which were two measurements done under the same conditions, but at a different time from the rest) showed the same characteristics described in detail for Fig. 4. In every case, except when the rf cavity voltage was 102 V, measurements of motion for f_0 greater than 1.031 680 MHz were very difficult. This may have been due to the circulating proton beam reaching an aperture limit as its energy increased. In the 102-V case, the results were very interesting in that they lack the expected symmetry around the $f_0 = 1.031\,680$ MHz. This implies that the damping force may not have the simple form assumed in Eq. (6). The deviation of the experimental results from the tracking results in all cases may also indicate a deficiency in the damping force model. Nevertheless, all measurements indicate that there exists a threshold $|v_{\rm rel}|$, beyond which the stable fixed point has bifurcated to a limit cycle.

2. *The limit cycle attractor*

While the computer tracking produces results that are consistent with the data, a more illuminating description of the motion and an explanation of threshold behavior can be obtained from the equation of motion with appropriate approximations. In this case, the general equation

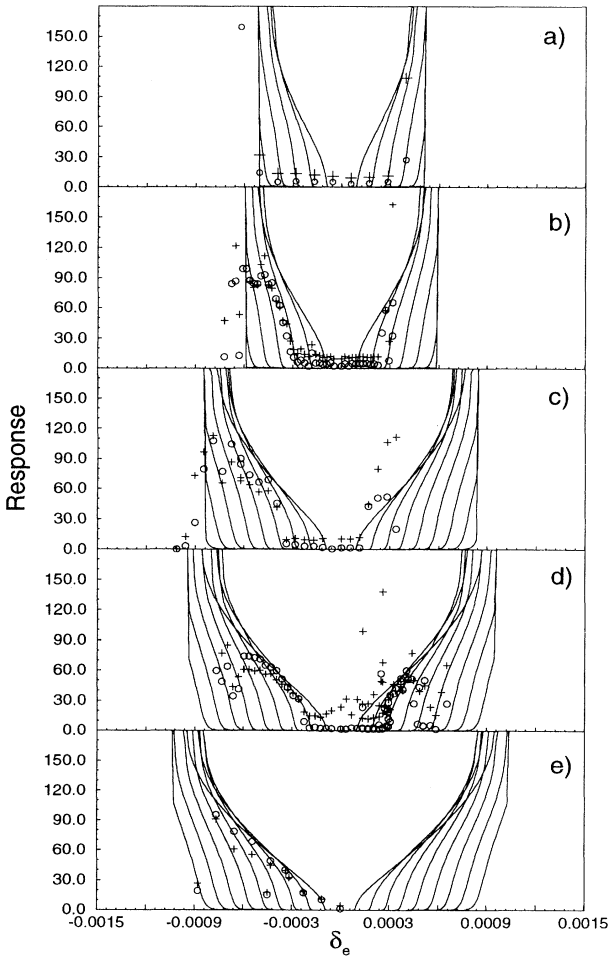

FIG. 5. Plots of $\hat{\phi}$ and $\hat{\delta}$ in degrees, similar to those of Fig. 4, vs δ_e, where δ_e is related to the rf cavity frequency via Eq. (20), for five different rf cavity voltages: (a) 32 V, (b) 40 V, (c) 78 V, (d) 102 V, and (e) 127 V.

of motion is

$$\ddot{\phi} + \frac{h\eta}{2\pi} f(\delta) + \nu_s^2 \sin\phi = 0, \tag{22}$$

where $f(\delta)$ is the damping force given by Eq. (6). Since the amplitude of the steady-state motion is small near the transition from a fixed point to the limit cycle bifurcation, we make the small amplitude approximation with $\sin\phi \approx \phi$. Let $x = \frac{\phi}{h\eta\Delta_e}$ be the new phase variable. From Eq. (2) the differential equation relating δ and ϕ is $\dot{\phi} = h\eta\delta$; thus $\dot{x} = \delta/\Delta_e$. The equation of motion becomes

$$\ddot{x} + \frac{2\alpha}{\omega_0} g(\dot{x} - \dot{x}_e) + \nu_s^2 x = 0, \tag{23}$$

where $\dot{x}_e = \delta_e/\Delta_e$ and $g(\zeta)$ is the kinematic function of Eq. (8).

Equation (23) is still a relatively complicated nonlinear differential equation, but as long as $2\alpha/\omega_0\nu_s$ is small, the location of the attractor can be determined by using a method called harmonic linearization [8]. This is done by assuming that the solution, after damping to the attractor, is given by

$$x = A\sin(\nu\theta). \tag{24}$$

Substituting the ansatz of Eq. (24) into Eq. (23), the resulting damping force is harmonic in time. We can expand the time-dependent damping kinematic factor in a Fourier series

$$g(\dot{x} - \dot{x}_e) = a_0 + \sum_{n=1}^{\infty} a_n \cos(n\nu\theta) + \sum_{n=1}^{\infty} b_n \sin(n\nu\theta), \tag{25}$$

where

$$a_0 = \frac{1}{2\pi}\int_0^{2\pi} g(\dot{x} - \dot{x}_e)\,d\theta, \tag{26}$$

$$a_n = \frac{1}{\pi}\int_0^{2\pi} g(\dot{x} - \dot{x}_e)\cos(n\nu\theta)\,d\theta, \tag{27}$$

$$b_n = \frac{1}{\pi}\int_0^{2\pi} g(\dot{x} - \dot{x}_e)\sin(n\nu\theta)\,d\theta. \tag{28}$$

Note that a_0, a_n, and b_n are all functions of $A\nu$ and δ_e/Δ_e. Now, the approximation of the harmonic linearization is to keep only the dominant terms in this expansion, which would be the dc term and the first harmonic term. In terms of x and $\dot{x}$, the damping force becomes

$$\frac{2\alpha}{\omega_0} g(x, \dot{x}) = 2\alpha_1\dot{x} + 2\nu_1\nu_s x + \nu^2 x_1, \tag{29}$$

where $\alpha_1 = a_1\alpha/(\omega_0\nu A)$, $\nu_1 = b_1\alpha/(\omega_0\nu_s A)$, and $x_1 = 2\alpha a_0/(\omega_0\nu^2)$, and likewise Eq. (23) becomes

$$\ddot{x} + 2\alpha_1\dot{x} + \nu^2(x - x_1) = 0, \tag{30}$$

where $\nu = \nu_s + \nu_1$, with $\nu_1 = 0$ for the linearized synchrotron motion. Note that α_1 corresponds to the average damping force over one complete synchrotron oscillation. If $\alpha_1 = 0$ for a given amplitude $A \neq 0$, then the limit cycle exists. Therefore, the amplitude A of the limit cycle attractor can be found by finding the location of the zeros in the function $\alpha_1(\frac{A\nu}{h\eta\Delta_e})$, or equivalently from the zeros in the function a_1. While closed form expressions for the functions in Eqs. (26)–(28) have not been obtained, these functions, and their zeros, were determined numerically.

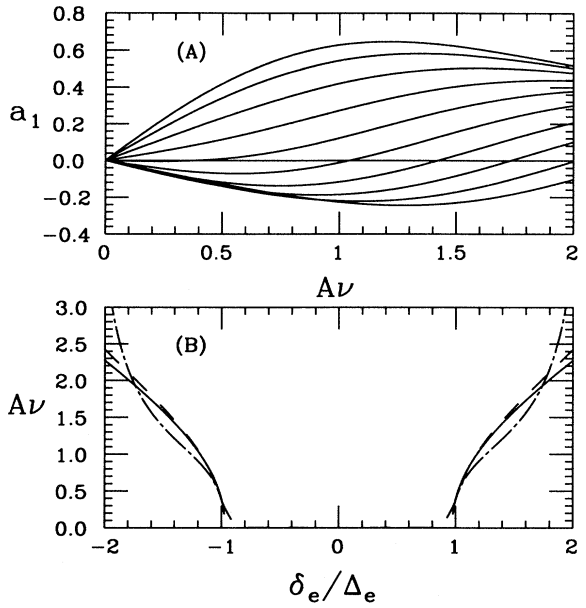

FIG. 6. (a) Plot of the function a_1 versus $A\nu$ for $\frac{\delta_e}{\Delta_e} = 0.2, 0.4, \ldots$ in intervals of 0.2. (b) Locations of the zeros for the curves in (a) versus $\frac{\delta_e}{\Delta_e}$ plotted as solid lines. The tracking result for $\Delta_e = 3 \times 10^{-4}$ of Fig. 4 is shown as dashed lines and the $A\nu$ obtained from Eq. (32) is shown as dash-dotted lines.

A plot of a_1 as a function of $A\nu$ for various values of δ_e/Δ_e is shown in Fig. 6(a). The locations of the zeros of a_1 as a function of the momentum offset δ_e/Δ_e is shown as solid lines in Fig. 6(b). For comparison, the location of the attractor as found from computer tracking of the difference equations is shown as a dashed line. This figure provides a qualitative explanation for the results obtained. As the fractional momentum offset of the electron beam is increased, the value of α_1 for small amplitude oscillations begins to decrease and eventually changes sign. The value of δ_e for which α_1 changes sign is where a driven, or maintained, oscillation first appears. This point happens to be at the δ_e, where $f(\delta_e)$ is an extremum, where the slope of the damping force changes sign. Once this occurs, the origin of the phase space becomes unstable. Thus once this condition is reached, the dynamics of this system resembles a system with negative resistance [9]. A bifurcation from a stable fixed point to a limit cycle, as in this case, is known as a Hopf bifurcation.

3. Heuristic explanation of the Hopf bifurcation

To further clarify the dynamics of the Hopf bifurcation, we can expand the nonlinear damping kinematic function of Eq. (23) in a Taylor series as

$$g(\dot{x}-\dot{x}_e)=\sum_{n=0}^{\infty} g_n \dot{x}^n, \tag{31}$$

where $g_n = \frac{1}{n!}\frac{d^n g(\zeta)}{d\zeta^n}\big|_{\zeta=-\dot{x}_e}$. Substituting the ansatz of Eq. (24) into Eq. (31), the conditions, up to the first harmonic, for the sustained limit cycle are $\nu=\nu_s$ and

$$g_1 A\nu + \frac{3}{4} g_3 (A\nu)^3 + \cdots = 0. \tag{32}$$

Neglecting all higher-order terms, we observe that Eq. (32) possesses a real solution when $g_1 g_3 < 0$. Thus the bifurcation occurs when the g_1 changes sign, i.e., at $\delta_e \approx 0.97\Delta_e$. The dash-dotted lines in Fig. 6(b) show the response amplitude $A\nu$ obtained from Eq. (32). They agree qualitatively with that of numerical simulations and that obtained from the harmonic linearization. It is interesting to note that the mechanism for the Hopf bifurcation arises from the cancellation between the negative resistance g_1 term and the higher-order dissipative term. The rf focusing potential provides the confinement for the sustained oscillations. The amplitude ϕ of the limit cycle is inversely proportional to the synchrotron tune, which agrees with numerical simulations shown in Fig. 5.

C. Observation and simulation of sustained dipolelike oscillations

With a Hopf bifurcation, particles would uniformly and incoherently populate a ring in the phase space. However, we often observed sustained dipolelike oscillations or a locally enhanced attractor instead of a uniformly distributed single limit cycle. Figure 7 shows the BPM sum signal observed from a fast sampling digital scope, which shows the longitudinal beam profile in a single path, for the rf frequency $f = 1.031\,03$ MHz. A double peaked feature with a slightly filled center region indicated that the beam was distributed in a ring. The peak phase amplitude of the ring is about 102°. The asymmetry in the peak current showed that a fixed point attractor might have appeared on the limit cycle.

Figure 8 shows the corresponding phase oscillations of the beam, recorded with our digitizing system [3], and the corresponding Poincaré map, which plots ϕ vs δ. We note that the maximum phase amplitude is about 80°, which is less than that measured from the BPM sum signal on the fast sampling scope discussed above. To observe the phase oscillation with the phase detector of our digitizing system, the beam must be largely a single bunch performing a dipolelike oscillation in the synchrotron phase space. Measuring the oscillation frequency, we found that the synchrotron frequency was 316 Hz.

A possible explanation for a sustained dipolelike synchrotron oscillation can be obtained from the superposition of the nonlinear damping force and a driven phase modulation, which may arise from power supply ripple, synchrobetatron coupling, or wake fields of the impedance. In the presence of phase modulation, the equations of synchrotron motion become

$$\delta_{n+1} = \delta_n - \frac{2\pi\nu_s^2}{h\eta}(\sin\phi_n - \sin\phi_s) - f(\delta_n), \tag{33}$$

$$\phi_{n+1} = \phi_n + 2\pi h\eta\delta_{n+1} + 2\pi\nu_m a\cos\nu_m\theta, \tag{34}$$

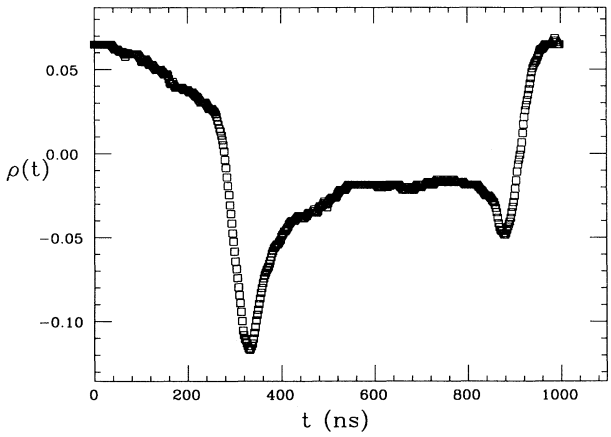

FIG. 7. Single trace of the longitudinal beam profile measured from a fast digital oscilloscope shows the uneven beam distribution on the limit cycle. Because of the nonuniform longitudinal distribution, our digitizing system can measure the phase oscillations of the dipolelike oscillations.

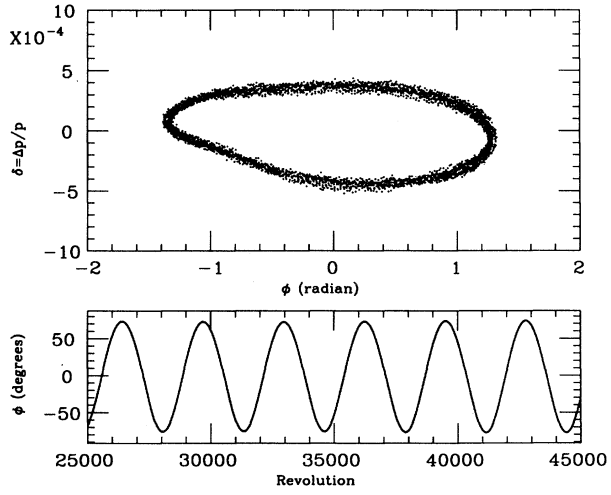

FIG. 8. Observed Poincaré map of the synchrotron oscillation for the sustained dipolelike oscillations shown in Fig. 7. The frequency of the dipolelike oscillation was 316 Hz.

where a and ν_m are, respectively, the modulation amplitude and the modulation tune. It is well known that the effect of the phase modulation will create a resonance island at the action J_r given by [4]

$$J_r \approx 8\left(1-\frac{\nu_m}{\nu_s}\right), \tag{35}$$

where the longitudinal action J is related to the phase amplitude by $J \approx \frac{1}{2}\hat{\phi}^2$. A characteristic feature of the harmonic phase modulation is that the maximum phase amplitude of the resonance island depends only on the modulation tune. Therefore, it will not change when the rf cavity frequency is altered. The fixed point attractor can be obtained from the Poincaré surfaces of section, where one phase space point is plotted every $1/\nu_m$ revolutions. Figure 9 shows an example of the Poincaré surfaces of section obtained from numerical simulations of Eqs. (33) and (34) with $a = 0.125°$, $\nu_m = 3.448\times10^{-4}$, and $\nu_s = 3.73\times10^{-4}$. Here the normalized fractional momentum deviation $\delta = -\frac{h|\eta|}{\nu_s}\frac{\Delta p}{p}$ is plotted against ϕ in radian. We observe that the Hopf bifurcation is swamped by the fixed point attractor generated by a very weak phase modulation.

It is worth noting that the measured phase amplitudes shown in Fig. 5 become nearly constant when the phase amplitudes reach a certain value. Before the onset of the Hopf bifurcation, the fixed point attractor originated from a small phase modulation could be washed away by the damping force of the electron cooling [4]. However, when the Hopf bifurcation occurs, the fixed point attractor of a small phase modulation is greatly enhanced, as shown in Fig. 9. We feel that this is a plausible explanation for the dipole character of the sustained oscillations; however, we cannot identify the source of 316 Hz.

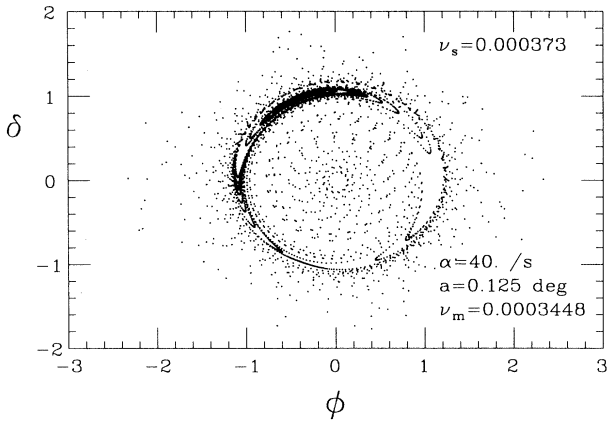

FIG. 9. Poincaré surfaces of section are plotted for the normalized phase space coordinates $\delta = -\frac{h|\eta|}{\nu_s}\frac{\Delta p}{p}$ vs ϕ in radians. They are obtained from numerical simulations of Eqs. (33) and (34) with parameters $\nu_s = 3.73\times10^{-4}$, $\nu_m = 3.448\times10^{-4}$, $a = 0.125°$, and $\alpha = 40\ \mathrm{s}^{-1}$. The nonlinear damping force produces a limiting cycle. In the presence of a phase modulation at a modulation tune near the synchrotron tune, a fixed point attractor is also created at the synchrotron amplitude given by Eq. (35).

D. The drag force of the electron cooling

Although our analysis assumed a specific kinematic form factor $g(\zeta)$ for the electron damping force, the threshold of Hopf bifurcation or limit cycle is generally independent of the small amplitude damping rate α and the specific form for the kinematic function for the damping force (see Sec. III B 3). To determine the damping rate α, we measured the small amplitude phase oscillations arising from voltage modulation of the electron acceleration column. On the other hand, the threshold of the Hopf bifurcation can be employed to determine the effective electron longitudinal temperature Δ_e. From our data, we obtained $\Delta_e \approx (3.1\pm0.9)\times10^{-4}$ and therefore the effective temperature was $kT_{\|\mathrm{eff}} \approx (2.2\pm1.0)\times10^{-3}$ eV.

It is instructive to compare the damping force determined from our experiments with the drag force measured through different means [5]. In storage rings with electron cooling, the cooling rate is measured by the drag force, which is defined as the energy loss or gain per unit length. Thus the drag force is related to the damping force by $\beta^2 Ef(\delta)/L_{\mathrm{cool}}$, where L_{cool} is the length of the electron cooling section. The drag force is generally proportional to the beam current of cooling electrons.

The drag force, with parameters $\alpha = 40$ Hz and $\Delta_e = 3.1\times10^{-4}$ shown as the solid line, is compared with data taken from p. 105 of Ref. [5] shown as various symbols in Fig. 10. These data were normalized to 0.75 A of electron current. The data, having the greatest slope in the asterisks, corresponded to the "magnetized cooling" condition, which was achieved by painstakingly aligning the electron beam with the proton beam at a very small electron current (e.g., 0.098 A) in order to minimize space charge depression. The drag force obtained from our experimental measurements is smaller than the magnetized cooling data of Ref. [5].

Our measured drag force also agrees well with Fig. 56 of Ref. [7]. Figure 11 compares our measured drag force (solid line) with those compiled in Fig. 56 of Ref. [7] shown as asterisks for the low energy antiproton ring (LEAR) data, circles for other machines (see Ref. [7] for detail), and squares for data taken from Ref. [5] at the IUCF Cooler Ring. Although the drag force data of these machines were measured at different energies, they behaved quite similarly. The drag force peaked at about 1.5×10^4 m/s for the optimized LEAR data, 2.8×10^4 m/s from our data, and about 4.5×10^4 m/s from the combination of all other data. The corresponding temperatures of the cooling electrons were about 0.0006 eV, 0.0022 eV, and 0.005 eV, respectively. Since all drag forces exhibit the characteristics of negative resistance, proton beams should experience Hopf bifurcation instability in all synchrotrons with electron cooling.

Although the damping force of Eq. (7) has a correct asymptotic form given by

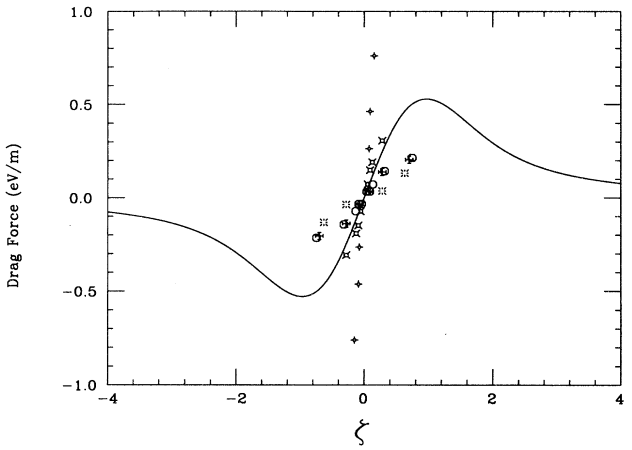

FIG. 10. The drag force (eV/m) obtained from our experiments is compared with that obtained previously by different methods [5] normalized to the electron current at 0.75 A. Different symbols corresponded to different machine conditions. The data, having the greatest slope in the asterisks, corresponded to the "magnetized cooling" condition, which was achieved by painstakingly aligning the electron beam with the proton beam at a very small electron current (e.g., 0.098 A) in order to minimize space charge depression. Note here that our result falls between the previously obtained magnetized and nonmagnetized cooling rate.

$$f(\delta) \sim \frac{3\pi^{3/2}\alpha\Delta_e^3}{\omega_0\delta^2},$$

the drag force, with the measured parameters $\alpha \approx 40$ s^{-1} and $\Delta_e = 3.1 \times 10^{-4}$, underestimates asymptotically the damping force of the empirical formula of Eq. (169) in Ref. [7] by a factor of 1.5. This discrepancy may arise

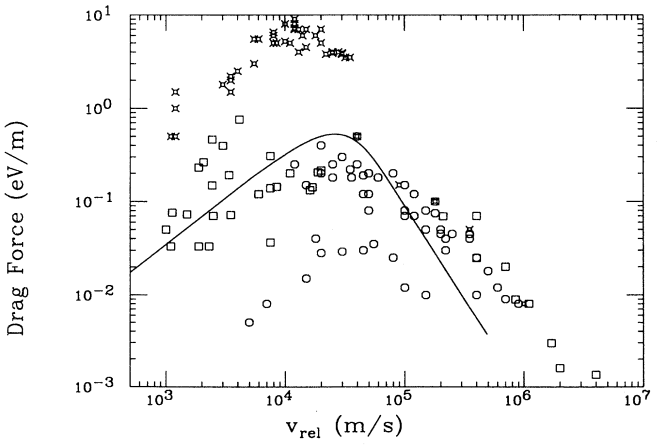

FIG. 11. The drag force (eV/m) obtained from our experiments (solid line) is compared with those compiled in Ref. [7]. The asterisks correspond to the optimized LEAR data, the squares are data taken from Ref. [5], and the circles are data of other machines compiled in Ref. [7].

from the oversimplified damping force used in our numerical simulations for the data analysis. A slower decrease in the electron cooling rate may also explain the smaller than expected response amplitude observed for large amplitude oscillations as in Figs. 4 and 5.

E. Comments on transverse Hopf bifurcation

Although we have studied only the nonlinear damping force in the longitudinal phase space, the result can be readily applied to the transverse electron cooling. Since the transverse damping force is also a nonlinear function of the relative transverse velocity [7], the Hopf bifurcation can occur when the relative transverse velocity is larger than that associated with the transverse temperature. A Hopf bifurcated beam may result in a more uniformly distributed beam in the coordinate space, which may benefit low energy storage rings in reducing the incoherent space charge tune shift.

IV. CONCLUSION

The longitudinal dynamics of a bunched beam with damping was explored when the damping force is harmonically modulated. The response of the beam to this modulation may prove useful as a diagnostic for determining the damping rate, as it was for this experiment. The harmonic modulation of the damping force was shown to produce driven motion, which has characteristics similar to rf phase modulation. Thus noise in a damping system may produce longitudinal emittance growth in the same way that phase noise in a rf system can.

We have made detailed studies of instabilities created by the nonlinear cooling force when the electron velocity differs from the proton velocity. We have shown that this instability can be explained as a maintained oscillation generated when operating with a relative velocity at which the damping force *decreases* with increasing momentum error, i.e., negative resistance. Because the maintained oscillation rises sharply and depends strongly on Δ_e, this effect may be used for determining the effective electron temperature Δ_e.

This phenomenon should also be an important consideration in injection schemes in which electron cooling is used to cool a proton beam at an energy different from the injected beam, since quite clearly it can have the unintended effect of heating the injected beam. More importantly, it may have an impact on the way in which the cooling electron and the proton beam energies are ramped. Cool-ramp-cool schemes have recently been developed for proton beam acceleration, in which protons are first injected, accumulated, and cooled to achieve small beam emittances, then the proton energy is ramped, and finally, the electron beam energy is brought to the speed of proton beam in order to achieving proper cooling at high energy. This process may encounter the negative resistance instability during the ramp manipulation. The question is how fast the Hopf bifurcation

develops. If the instability growth rate, which unfortunately seems to be proportional to α, is faster than the ramping rate, the beam particles will be unstable. On the other hand, if the ramping rate is larger than the instability growth rate, then the effect of nonlinear cooling force plays little role in diluting the phase space during the acceleration. It is therefore worth studying the Hopf bifurcation growth time. The degree to which this phenomenon may affect these operations requires further studies and awaits a more sophisticated treatment of the motion that can predict the amplitude of the transient and its growth time.

ACKNOWLEDGMENTS

We wish to thank S. Nagaitsev and J. Ellison for their helpful comments. This work was supported by grants from the NSF, No. PHY-9221402, and the DOE, No. DE-FG02-93ER40801.

[1] R.E. Pollock, Annu. Rev. Nucl. Sci. **41**, 357 (1991).
[2] E.M. McMillan, Phys. Rev. **68**, 143 (1945); V.I. Veksler, C. R. Acad. Sci. USSR **43**, 329 (1944); **44**, 365 (1944).
[3] S.Y. Lee *et al.*, Phys. Rev. Lett. **67**, 3768 (1991); D.D. Caussyn *et al.*, Phys. Rev. A **46**, 7942 (1992); M. Ellison *et al.*, Phys. Rev. E **50**, 4051 (1994).
[4] M. Ellison *et al.*, Phys. Rev. Lett. **70**, 591 (1993); H. Huang *et al.*, Phys. Rev. E **48**, 4678 (1993); D. Li *et al.*, *ibid.* **48**, R1638 (1993); M. Syphers *et al.*, Phys. Rev. Lett. **71**, 719 (1993); Y. Wang *et al.*, Phys. Rev. E **49**, 1610 (1994).
[5] Tim Ellison, Ph.D. thesis, Indiana University, 1990.
[6] R.E. Pollock *et al.*, Nucl. Instrum. Methods Phys. Res. A **330**, 380 (1993).
[7] H. Poth, Phys. Rep. **196**, 135 (1990).
[8] I. Huntly and R.M. Johnson, *Linear and Nonlinear Differential Equations* (Halsted, New York, 1983), pp. 166–168.
[9] A.B. Pippard, *The Physics of Vibration* (Cambridge University Press, New York, 1978), pp. 306–342.